A hybrid modelling approach for characterizing hole shrinkage mechanisms in drilling Ti6Al4V under dry and cryogenic conditions

Hongguang Liu, Hélène Birembaux, Yessine Ayed, Frédéric Rossi, Gérard Poulachon, Hélène Birembaux

https://doi.org/10.1007/s00170-021-08229-2

A hybrid modelling approach for characterizing hole shrinkage mechanisms in drilling Ti6Al4V under dry and cryogenic conditions

Hongguang Liu[1] · Hélène Birembaux[1] · Yessine Ayed[2] · Frédéric Rossi[1] · Gérard Poulachon[1]

Abstract

Hole shrinkage is a common phenomenon in drilling difficult-to-cut materials like Ti6Al4V due to their poor thermal properties and high elasticity, which can lead to increase in tool wear and decrease in surface integrity. In this study, an in-depth analysis of hole shrinkage mechanism is carried out through a hybrid modelling approach for both dry and cryogenic cutting conditions. The plastic deformation induced by chip formation and tool-workpiece interaction is treated as equivalent thermomechanical loads, and heat convection conditions are described along tool path in order to perform details in heat transfer process for both cases. Quantitative analysis is presented through numerical simulation and experimental data of temperature and deformation along hole contour to analyze deformation components in order to reveal the hole shrinkage mechanism. Additional interactions between cutting tool and workpiece material are induced by recovery of elastoplastic deformation, and plastic portion is a more devastating factor in tool wear and surface damage induced by hole shrinkage. This study presents an in-depth and fundamental understanding of the hole shrinkage mechanism through a hybrid modelling approach, which can characterize heat transfer process during machining for both dry and cryogenic conditions, and simulation of this fully coupled thermomechanical cutting process with supply of coolants was rarely reported in previous research. The results show that plastic deformation induced hole shrinkage can enhance the interaction between workpiece material and cutting tool, and cryogenic assistance presents a good performance in restricting this kind of phenomenon. The related results could be used to optimize strategies of eliminating hole shrinkage with cryogenic assistance in industrial applications.

Keywords Cryogenic machining · Hole shrinkage · Drilling · Hybrid approach · Ti6Al4V

Nomenclature

D	The drill diameter (mm)
l	The height of drill tip (mm)
d	Projection distance of nozzle (mm)
ϕ	The nozzle diameter (mm)
φ_2	The projection angle (°)
A, B, C	VPL model parameters regarding strain hardening
n	VPL model parameter regarding strain rate hardening
v	VPL model parameter regarding thermal softening
T_r	Reference temperature (K)
h	The height of contact (mm)
w	The width of margin (mm)
Δh	Incremental height per tooth per revolution (mm/r)
σ	Normal stress (MPa)
τ	Tangential stress (MPa)
μ_l	Friction coefficient of main edge
μ_h	Friction coefficient of margin
F_r	Radial force (N)
F_t	Tangential force (N)
F_f	Feed force (N)
Λ_1	Percentage of shearing energy transformed into heat
Λ_2	Percentage of heat produced during chip formation and transformed into machined surface
Λ_3	Heat partition coefficient at the interface of tool-workpiece

✉ Hongguang Liu
hongguang.liu@ensam.eu

[1] Arts et Metiers Institute of Technology, LaBoMaP, Université Bourgogne Franche-Comté, HESAM Université, Rue Porte de Paris, 71250 Cluny, France

[2] Arts et Metiers Institute of Technology, LAMPA, HESAM Université, 2 Boulevard du Ronceray, 49035 Angers, France

$D_{l\text{-flux}}$	Heat flux intensity of main cutting edge area (W/mm^2)
$D_{h\text{-flux}}$	Heat flux intensity of margin area (W/mm^2)
$\varepsilon, \beta, \gamma, \delta, i, j, k, m$	Controlling parameters for calculating heat convection coefficient
ϕ_{ref}, P_{ref}, D_{ref}, α_{ref}	Referencing values of nozzle diameter, projection pressure, projection distance and projection angle
P	Driven pressure of LN_2 applied in experiments (Bar)
α	Projection angle of LN_2 (°)
a, b	Intermediate variables for calculating distribution of heat convection coefficient
t	The current time step during machining process (s)
$x(t), y(t), z(t)$	The coordinates of margin along x-, y-, and z-axis at the current time t
T_N	Time required for a single rotation (s)
z_0	Initial position of tool along z-direction (mm

1 Introduction

Ti6Al4V alloys are widely used in aerospace industries due to their high strength-to-weight ratio, excellent corrosion resistance, and good mechanical properties at high temperatures [1, 2]. However, the extremely low thermal conductivity, high elasticity, etc. make it a typically difficult-to-cut material. For Ti6Al4V, it is usually machined as structural components for aircrafts, which requires to be assembled with other components, and riveting is the most popular method for this purpose, which makes drilling one of the most common techniques applied for Ti6Al4V.

During drilling of difficult-to-cut materials like Ti6Al4V, severe tool wear [3, 4] and hole contour variation like cylindricity and circularity [5] induced by accumulation of thermal effects are main issues. Tool wear can significantly increase the costs of machining process and decrease surface quality, which will finally influence hole geometries and service performance of components. Meanwhile, hole shrinkage will enhance the interaction between cutting tool and workpiece material, which will further speed up tool wear, decrease surface quality, and can also lead to burr formation at the entry and the exit of the hole [6]. To overcome these issues, good choices of cooling strategies are necessary. The concept of cryogenic cutting was firstly raised by Uehara and Kumagai [7], and then developed by Hong et al. [8–10], which utilizes liquid nitrogen (LN_2) with extremely low temperature to cool down the cutting zones. Since it comes out, it attracts a lot of concerns from researchers all over the world and is becoming more and more popular due to its excellent performance in reducing thermal induced tool wear and significant improvement in economic and environmental perspectives [8, 11, 12]. Ayed et al. [13] carried out a series of experiments to investigate the impact of flow rates and pressures of cryogenic liquids on tool wear and residual stress during Ti6Al4V machining, which shows a good performance of LN_2 in improving tool life and surface integrity. Then, Stampfer et al. [14] investigated the cooling effects of LN_2 with respect to supply pressure and subcooler usage for turning, which was used to identify the reliable cooling strategies. Merzouki et al. [5, 15] investigated the contact height induced by hole shrinkage and proposed a method for experimentally measuring the radial forces induced by hole shrinkage; however, in-depth analysis of hole shrinkage mechanisms were not presented. Kaynak et al. [16] showed that cryogenic assistance can help to increase the machinability of workpiece material. Shokrani et al. [17] investigated machining of Ti6Al4V under different cooling conditions, which shows that cryogenic cutting can significantly improve the surface integrity compared to dry and flood conditions. Pusavec et al. [18] analyzed the influence of nitrogen phases on the performance of heat transfer in surfaces during cutting process, which provides a basement for more detailed modeling of cryogenic cutting. Guo et al. [19] carried out experiments through micro-pillar compression, which shows that the constitutive behaviors and wear resistance of machined surface can be significantly strengthened by cryogenic machining process. Although the experimental investigations present some basic comprehension of cryogenic cutting process, quantitative analysis is still required for fundamental understandings of thermomechanical conditions in cryogenic cutting.

For quantitative description of fully coupled thermomechanical process and related material behaviors, numerical simulation methods like finite element method (FEM) and related coupled methods are always used [20]. Salame et al. [21] used FEM to analyze chip formation process and transfer data to computational fluid dynamics (CFD) for calculation of temperature, which performs a good description of liquid–gas transformation in cutting; however, cutting process and heat transfer process are calculated separately, while these processes occur simultaneously for actual conditions. Rotella and Umbrello [22] simulated cryogenic cutting process with a simplified method by applying a heat transfer coefficient between workpiece and environment, which is lack of accuracy in description of the heat transfer process. Dix et al. [23] used a 3D modeling method to carry out drilling simulation with cryogenic assistance; however, their simulation lasts only for 2.5 revolutions due to the extremely long calculation time, which cannot reach the stable conditions of thermomechanical loads, and only transient states can be analyzed as a result. Imbrogno et al. [24, 25] also

presented a 3D simulation method with application of commercial software Deform 3D due to its convenience in performing 3D machining simulations; however, their methods can only be applied when heat transfer occurs between LN_2 and cutting tool, which cannot express the interaction between workpiece material and LN_2, as it can be only applied for a fixed surface. Shi et al. [26] proposed a hybrid modeling approach to combine simulation results of CFD and FEM to perform 3D turning simulation with cryogenic assistance, and a heat exchange window with simplified cylinder shape was applied to describe the cooling process of the rake face induced by LN_2. This method cannot give an accurate description of the interaction between LN_2, cutting tool, and workpiece. As a result, better methods need to be developed for cryogenic cutting process in order to carry out in-depth understandings of the inner mechanisms.

In this paper, a hybrid modeling approach based on FEM is developed to analyze the variation of deformation conditions along hole contour during drilling in order to characterize the mechanisms of hole shrinkage. The thermomechanical loads produced by the interaction between drill tip and workpiece material are determined through an equivalent approach, which includes both plastic deformation-based loads and friction-based loads. The heat exchange during this whole process is described with respect to the detailed helix path of drill and coolants movement. This method is then applied to analyze the mechanisms of hole shrinkage in drilling under dry and cryogenic conditions, and the results are validated against experimental data. Cryogenic drilling presents an advantage of improving surface integrity through restricting hole shrinkage and reducing excessive deformation. These results can be further used for parameter optimization of drilling process.

2 Modeling approach

For 3D simulation of drilling process by FEM, the complicated chip formation and material removal process are very time-consuming, which is the key limitation for performing simulations illustrated by Dix et al. [23]. In this study, the main concern is the final contour of the hole surface, especially the central part of the hole as the cutting loads are more stable within this area. As a result, the complicated chip formation process can be regarded as thermomechanical loads applied on it, which can be equivalent and simplified through an analytical model proposed by Valiorgue et al. [27–29]. This method is dependent on experimental data for parameter identification of thermomechanical loads; meanwhile, the description of heat convection conditions requires to be identified by experimental parameters as well, and these data are then transferred as the input for numerical simulation by FEM, the schematic is as shown in Fig. 1.

This approach is composed of three sections: firstly, data acquisition through experiments, then data processing and parameter identification are proceeded for obtaining equivalent thermomechanical loads and heat convection conditions, and finally the loads and boundary conditions are applied for numerical simulation, detailed explanation of calculation for all the related inputs are described in "Sect. 4." This approach could improve the calculation efficiency by eliminating the simulation of time consuming chip formation procedure and related distortions of meshes. Moreover, for cryogenic cutting condition, it can provide a more detailed and precise description of the heat convection process between workpieces and coolants than normal simulations as illustrated in references [21–23, 26], which will be introduced in details in "Sect. 3, 4 and 5."

3 Experimentation

Experiments were carried out through a 3-axis milling machine (model: HURON KX10) with removable carbide inserts (model: ISCAR ICM 120 IC908). The geometry of the insert and location of nozzles are presented as shown in Fig. 2, and the detailed parameters of drill geometry can be found in Table 1.

The LN_2 used for cryogenic assistance was stored in a tank with internal pressure of 10 bars, which was driven to the cutting zone through the spindle and internal lubricant holes of the drill, which are marked as nozzles in Fig. 2. Cutting forces and torques were measured together with application of rotary dynamometer (model: KISTLER 9123C) and fixed dynamometer (model: KISTLER 9257B). A bi-plate method raised by Merzouki et al. [5] was used to obtain the radial forces induced by hole shrinkage. The schematic of the set-up is as shown in Fig. 3.

The contact height induced by hole shrinkage between margins and hole surface during the whole-drilling process was determined due to the variation of cutting torques and feed forces due to high elasticity of Ti6Al4V at the exit of the drilling hole through the method proposed by Merzouki et al. [15]. Cutting experiments were performed with same parameters for both dry and cryogenic cases, which were cutting speeds V_c of 30 m/min and feed f of 0.08 mm/r, the whole thickness of the plate is 25.5 mm. Each experiment was carried out for 5 times to prove the repeatability, and cutting temperatures were measured with K-type thermocouples installed at 1 mm from the hole surface, as shown in Fig. 3.

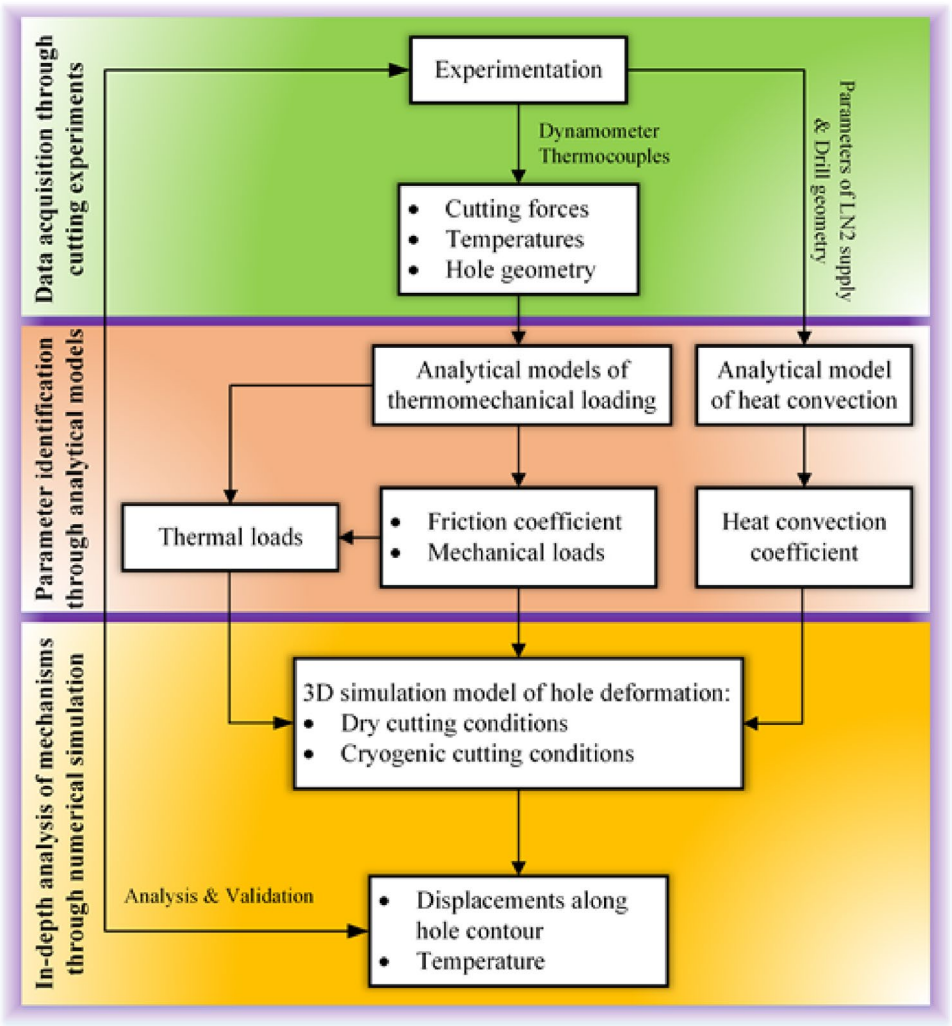

Fig.1 Schematic of the hybrid modeling approach

4 Parameter identification for numerical modeling

4.1 Material model

Constitutive behavior is a key factor influencing the material deformation during cutting process; in this paper, a modified constitutive model of voce power law (VPL) model raised by Shi et al. [26] is adopted, which has been successfully applied in simulations of cryogenic cutting conditions [26], and the model can be expressed as follows:

$$\sigma = [A - B\exp(C\varepsilon)](\frac{\dot{\varepsilon}}{\dot{\varepsilon}_0})^n(\frac{T}{T_r})^\upsilon \quad (1)$$

where A, B, and C are all the controlling parameters for the strain hardening behavior, n is the parameter describing the strain rate effects and υ the parameter for thermal effects. $\dot{\varepsilon}_0$ is the reference strain rate and T_r the reference temperature; for this model, the unit used for temperature should be Kelvin. From the publication of Shi et al. [26], model parameters were not calibrated for material behaviors at low temperature; as a result, they are re-calibrated against experimental data for both high temperature behaviors from Ramirez [30] and low temperature behaviors from Follansbee and Grey [31], as shown in Table 2.

The calibration of VPL model with parameters listed in Table 2 is shown in Fig. 4, which shows a good agreement with experimental data at both high and low temperature ranges, and it is also acceptable for high strain rate applications, although this modeling approach will not preset extremely high strain rate due to the lack of chip formation process. These parameters were fitted against experimental data to characterize good results in a large temperature range, so that it can be used for both cases of dry cutting condition and cryogenic cutting condition. This model is then implemented for numerical simulations as a subroutine for both conditions.

Moreover, Young's modulus and thermal properties of Ti6Al4V are used as temperature-dependent parameters

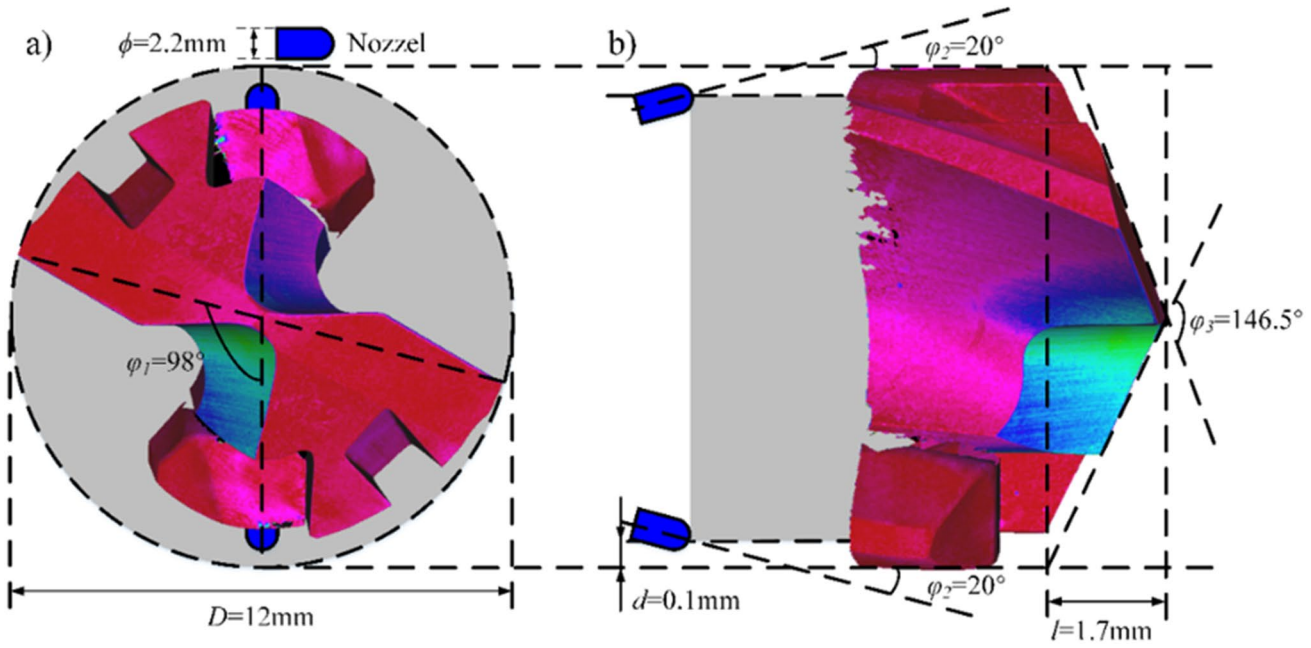

Fig.2 Geometry of the drill insert, **a** top view and **b** side view, where D shows the drill diameter, l the height of drill tip, d the gap between drill and hole surface, ϕ the nozzle diameter, φ_1 the angle between nozzle and cutting area, φ_2 the angle between nozzle and drill axis, and φ_3 the angle between main cutting edges from cylindrical section

Table 1 Geometrical parameters of drill

Parameter	Symbol	Value
Drill diameter (mm)	D	12
Nozzle diameter (mm)	ϕ	2.2
Phase angle between nozzle and margin (°)	φ_1	98
Projection angle of nozzle (°)	φ_2	20
Tip angle of drill bit (°)	φ_3	146.5
Height of drill tip (mm)	l	1.7
Projection distance of nozzle (mm)	d	0.1

with values referenced from Mills [32] and Ramirez [30], as shown in Table 3.

Meanwhile, for cryogenic region, the temperature-dependent material properties will be changed as well, which will have an influence on the final cutting performance. Marquardt et al. [34] and Ziegler et al. [35] provided a database for characterizing thermal properties of material at cryogenic conditions with temperatures ranging from 20 to 300 K (− 253 to 27 °C), and the related properties of Ti6Al4V alloys can be found in Table 4.

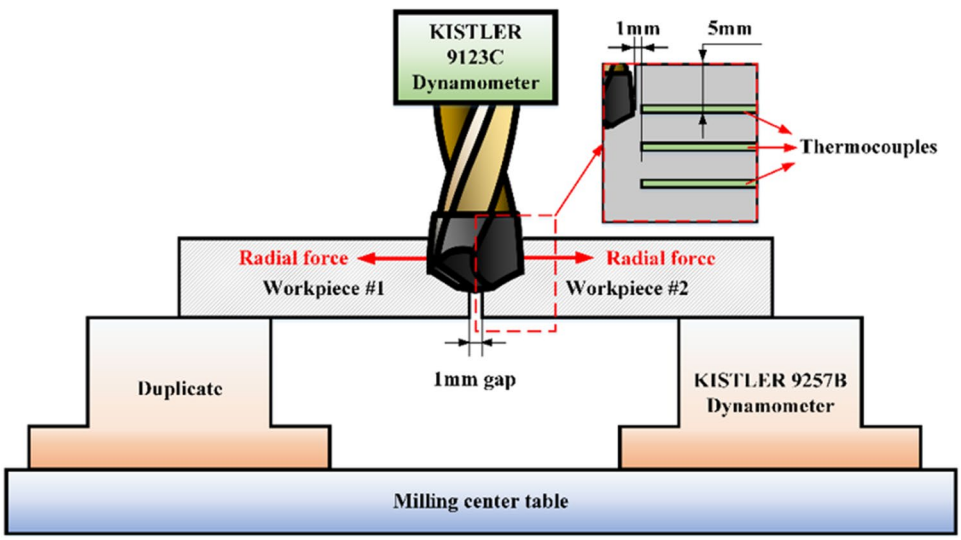

Fig. 3 Description of experimental set-up [5]

Table 2 Calibrated parameters of VPL model for Ti6Al4V

Parameter	A/MPa	B/MPa	C	n	υ	$\dot{\varepsilon}_0/s^{-1}$	T_r/K
Value	1475.2	327.6	− 3.02	0.012	− 0.7822	0.001	293.15

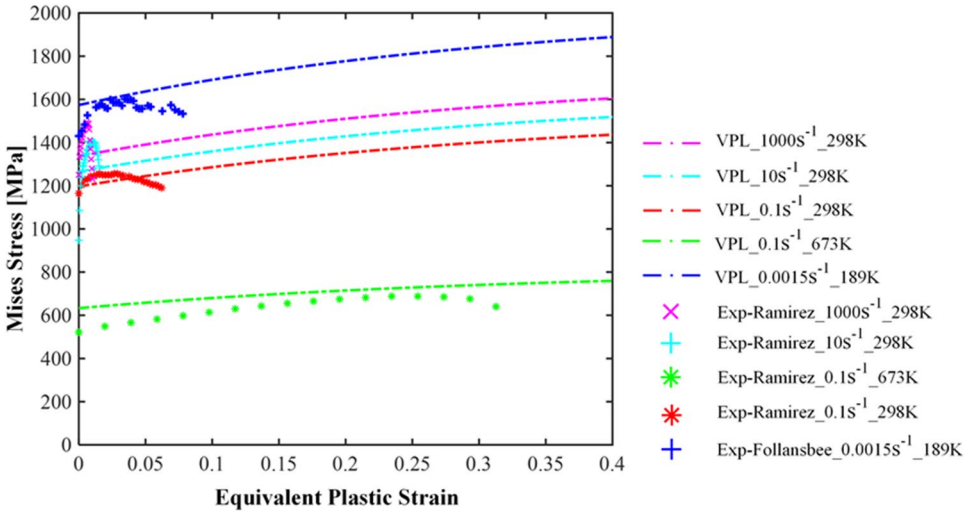

Fig. 4 Calibration of constitutive behaviors for Ti6Al4V [30, 31]

Table 3 Temperature-dependent properties of Ti6Al4V at high temperature range [30, 32, 33]

Temperature (°C)	Young's modulus (GPa)	Specific heat (J/kg•K)	Thermal conductivity (W/m•K)	Thermal expansion ($\times 10^{-6}$ m/m•K)
100	115.27	562	7.45	8.78
200	110.07	584	8.75	9.14
300	105.85	606	10.15	9.49
400	100.35	629	11.35	9.85
500	94.95	651	12.6	10.21
600	89.54	673	14.2	10.57
700	84.08	694	15.5	10.93
800	79.93	714	17.8	11.28
900	76.49	734	20.2	11.64
1000	76.09	754	22.7	12

4.2 Mechanical loads

During drilling process, the mechanical loads applied on hole surface are mainly due to the additional interactions between drill and hole surface induced by hole shrinkage, which can be decomposed into radial direction and tangential direction. For radial direction, the loads can be used as normal pressure, and shear stress for tangential direction. As mechanical loads applied on hole surface are primarily induced by the hole shrinkage between margin and hole surface, the normal pressure and shear stress applied on the surface can be calculated through the radial and tangential cutting forces, as illustrated in Fig. 5.

From Fig. 5, F_r shows the radial force and F_t the tangential forces. These forces can be transferred from forces in x- and y-directions that can be directly measured through the dynamometer with respect to phase angle during the rotation through the utilization of the set-up shown in Fig. 3. The raw data of measured cutting forces can be found in Fig. 6.

Meanwhile, the maximum value of cutting forces will appear at the tool tip between margin and main cutting edge, and the cutting forces along radial and tangential directions can be decomposed along margin with the method proposed by Poutord et al. [4], then the mechanical loads can be determined by the following equations:

$$\begin{cases} \sigma = \dfrac{F_r}{w \cdot \Delta h} \\ \tau = \dfrac{F_t}{w \cdot \Delta h} \end{cases} \tag{2}$$

where w is the width of the margin, which equals to 0.85 mm in this study, and Δh the incremental height for each feed, which can be described as $\Delta h = f/2$, as the drill used in this study has two flutes. According to Merzouki et al. [15], the heights of contact for dry cutting condition and cryogenic cutting condition are experimentally identified as 1.36 mm and 0.48 mm, respectively; as a result, the mechanical loadings induced by hole shrinkage along the margin can be described as a linear distribution as shown in Fig. 7.

Table 4 Material properties of Ti6Al4V at low temperature range [30, 34, 35]

Temperature (°C)	Young's modulus (GPa)	Specific heat (J/kg•K)	Thermal conductivity (W/m•K)	Thermal expansion ($\times 10^{-6}$ m/m•K)
− 253	-	8.21	0.8426	− 86.8
− 248	-	16.04	1.5763	− 69.44
− 223	-	99.52	2.4107	− 34.16
− 193	-	228.85	3.5308	− 20.1375
− 173	-	301.03	3.8045	− 15.16
− 123	-	415.5	4.6215	− 7.94
− 73	-	478.13	5.7498	− 3.93
− 23		513.72	6.5931	− 1.415
2	119.21	530.05	6.9826	− 0.524
22	118.3	538.84	7.4145	8.5

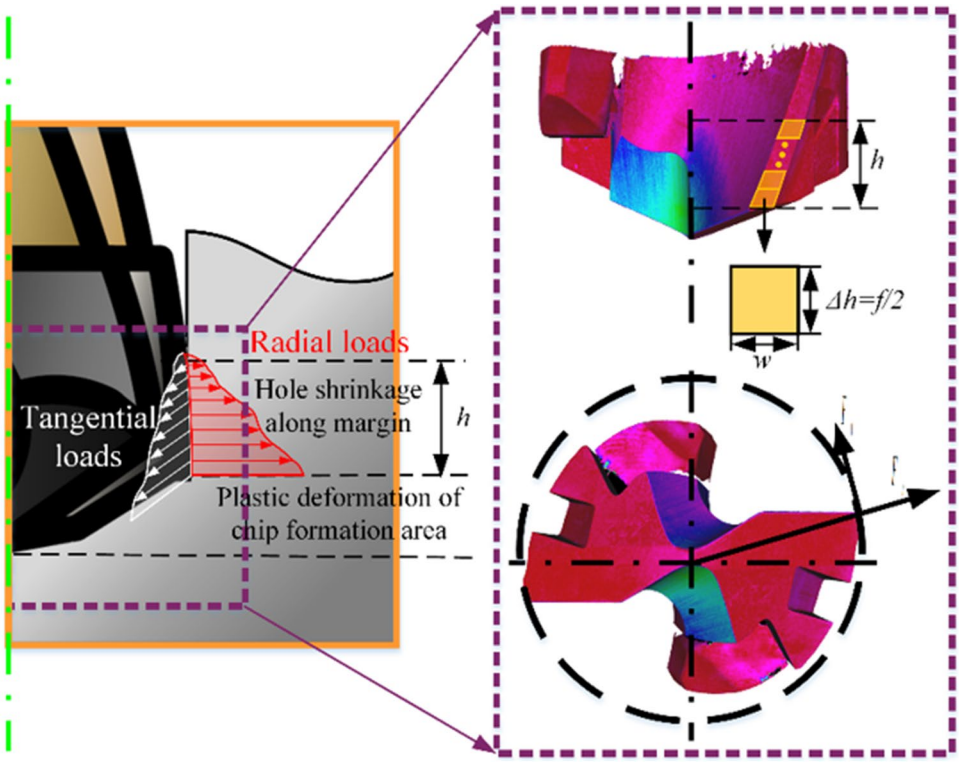

Fig. 5 Mechanical loads induced by hole shrinkage on the cylindrical surface

4.3 Thermal loads

Thermal loads are mainly described as a heat flux intensity, which are always induced by plastic deformation of material removal process during chip formation, and friction between cutting tool and workpiece material. When the drill proceeds to feed, the main resistance from material can be regarded as feed forces and radial forces from cylindrical perspective. Meanwhile, the heat flux applied on the hole surface can be divided into three sections as a result, which are all primarily induced by mechanical loadings, and a similar shape of heat flux distribution was presented by Faverjon et al. [36] with consideration of contact length between drill and workpiece material. As a result, the distribution of heat flux intensity is assumed to characterize a similar linear distribution as mechanical loads, as shown in Fig. 8.

From Fig. 8, main contributions of heat flux applied on hole surface are induced by the hole shrinkage with margin penetrated into the workpiece, while the contribution from plastic deformation of chips along main cutting edge is limited as its main transfer direction is consistent with feed direction. Here, h shows the height of contact between the margin and the workpiece, and d_c shows the penetration height of main edge induced by hole shrinkage. With

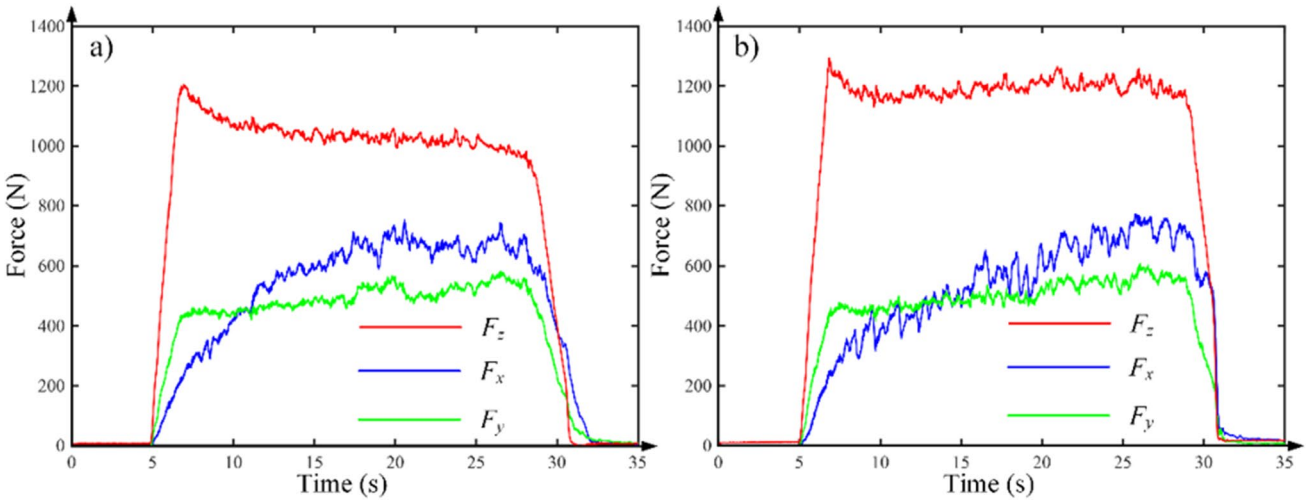

Fig. 6 Cutting forces evolution under different cooling conditions with cutting speed 30 m/min and feed 0.08 mm/r, **a** dry and **b** cryogenic

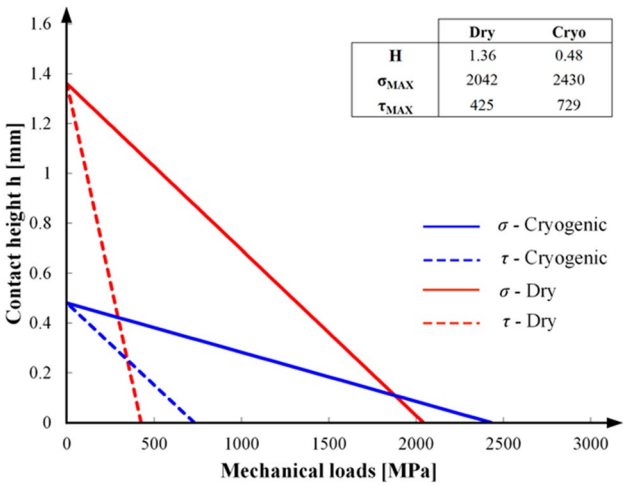

Fig. 7 Mechanical loads with respect to contact height of radial and tangential directions induced by hole shrinkage along margin [15]

analysis shown in Fig. 8, heat flux can be calculated according to local cutting forces in different areas, as a result, cutting forces require to be decomposed according to Mondelin et al. [29] as follows:

$$F_f = F_{f1} + F_{f2} \tag{3}$$

$$F_r = F_{r1} + F_{r2} \tag{4}$$

$$F_{r1} = \mu_l F_{f1} \tag{5}$$

$$F_{f2} = \mu_h F_{r2} \tag{6}$$

where μ_l and μ_h represent the friction coefficients along main cutting edges and margins, respectively, and F_f and F_r are the feed force and radial force, respectively. These equations can be further derived as follows:

$$F_{f1} = \frac{1}{1 - \mu_l \cdot \mu_h}(F_f - \mu_h \cdot F_r) \tag{7}$$

$$F_{f2} = \frac{\mu_h}{1 - \mu_l \cdot \mu_h}(F_r - \mu_l \cdot F_f) \tag{8}$$

Then, the maximum values of heat flux intensity within different areas can be estimated through [29]:

$$D_{l-\text{flux}} = \frac{F_{f1} \cdot V_C}{60 \cdot l \cdot \Delta w}\Lambda_1\Lambda_2 \tag{9}$$

$$D_{h-\text{flux}} = \frac{F_{f2} \cdot V_C}{60 \cdot h \cdot \Delta w}\Lambda_3 \tag{10}$$

where l and h are the penetration distance of main cutting edge and contact height, respectively, and Δw the incremental width between margin and hole surface for each time increment, which is regarded as the same value with feed in this study. The number 60 in the equation is used for unit transfer as cutting speed has a unit of m/min here. Λ_1 is the percentage of shearing energy transformed into heat and Λ_2 the percentage of heat produced by plastic deformation in chip formation transformed into machined surface. According to Shi et al. [37], the values of Λ_1 and Λ_2 can be used as 0.85 and 0.1 for dry cutting condition, respectively, and for cryogenic condition, we assume the parameters the same as dry condition due to the low percentage. Λ_3 is the heat partition coefficient at the interface, which shows the percentage of generated heat flux conducted to the machined

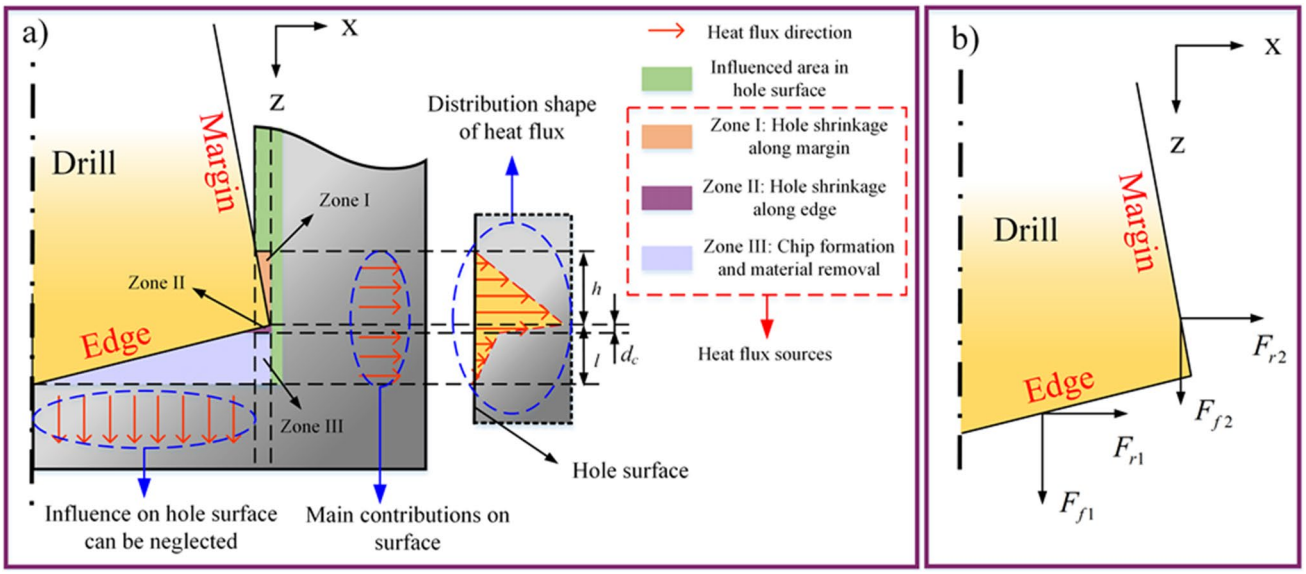

Fig. 8 Heat flux sources and shape of distribution applied on hole surface, **a** schematic of heat flux distribution, **b** cutting forces from cylindrical section

surface. Rech et al. [38, 39] presented the characterization of this coefficient for machining Ti6Al4V with both dry and cryogenic conditions through friction tests. For dry cutting condition, it is assumed that heat is conducted by tool-chip and workpiece; while for cryogenic condition, most heat is removed by coolants, so the same heat partition percentage is used for cutting tool and workpiece. As a result, the coefficients Λ_3 are calculated as 0.45 and 0.15 for dry and cryogenic conditions according to Courbon et al. [39], respectively. As heat flux is calculated from mechanical loads, a same linear distribution as mechanical loads described in "Sect. 4.2" is applied for heat flux, as illustrated in Fig. 8, which is dependent on drill geometry and height of contact along margins. Then, the distribution of heat flux intensity can be obtained as shown in Fig. 9.

4.4 Heat convection coefficient

For cryogenic cutting condition, a precise description of heat convection coefficient is essential for characterizing the heat transfer process between cryogenic coolant LN_2 and workpiece. When the contact between LN_2 and workpiece occurs, the distribution of heat convection coefficient is not uniform, which will be a Gaussian distribution instead, as reported by Lequien et al. [40]. According to their research, the values of heat convection coefficient are always dependent on nozzle diameter ϕ, projection pressure P, projection distance D, and projection angle α, which can be described as follows [40]:

$$h(f(t)) = a \cdot \exp\left(\frac{-f^2(t)}{2b^2}\right) \tag{11}$$

$$a = A \cdot \left(\frac{\phi}{\phi_{\text{ref}}}\right)^{\varepsilon} \cdot \left(\frac{P}{P_{\text{ref}}}\right)^{\beta} \cdot \left(\frac{D}{D_{\text{ref}}}\right)^{\gamma} \cdot \left(\frac{\alpha}{\alpha_{\text{ref}}}\right)^{\delta} \tag{12}$$

$$b = S \cdot \left(\frac{\phi}{\phi_{\text{ref}}}\right)^{i} \cdot \left(\frac{P}{P_{\text{ref}}}\right)^{j} \cdot \left(\frac{D}{D_{\text{ref}}}\right)^{k} \cdot \left(\frac{\alpha}{\alpha_{\text{ref}}}\right)^{m} \tag{13}$$

where ε, β, γ, δ, i, j, k, and m are all controlling parameters, while ϕ_{ref}, P_{ref}, D_{ref}, and α_{ref} are referenced values of nozzle diameter, projection pressure, projection distance, and projection angle, respectively. The function $f(t)$ characterizes the coordinates of tool tip. The parameters for characterizing the interaction between LN_2 and Ti6Al4V are shown in Table 5.

In this study, the projection pressure is 3 bars, and the geometrical parameters of nozzle diameter, projection distance, and projection angle can be obtained through measuring geometrical parameters of the drill shown in Fig. 2, which are 2.2 mm, 0.1 mm, and 70°, respectively. As a result, the distribution of heat convection coefficient in this study can be described as shown in Fig. 10.

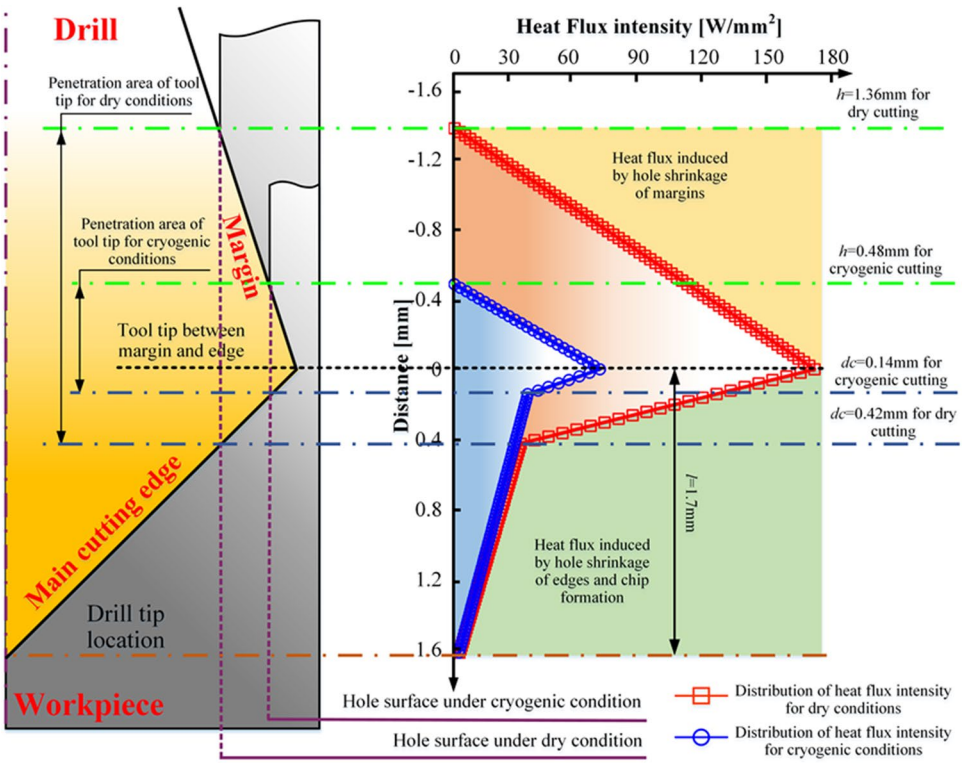

Fig. 9 Distribution of heat flux on the hole surface under dry and cryogenic conditions

Table 5 Parameters for identifying heat convection coefficient [40, 41]

Parameter	Value	Parameter	Value	Parameter	Value
A (W/m^2•K)	23,086	S	3.069	ϕ_{ref} (mm)	6
ε	0.521	i	0.223	P_{ref} (bar)	10
β	0.212	j	0.048	D_{ref} (mm)	50
γ	0	k	0	α_{ref} (°)	3
δ	0	m	0		

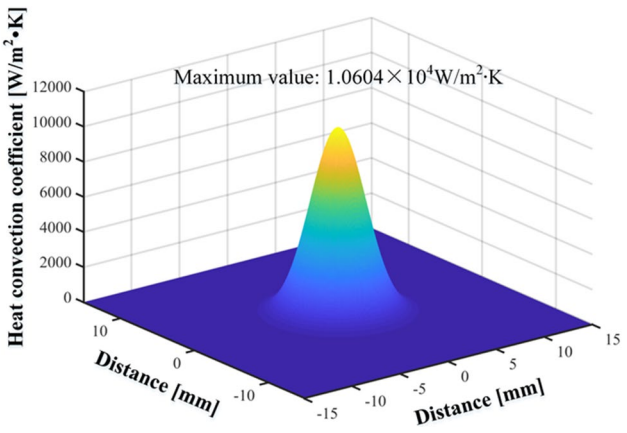

Fig. 10 Distribution of heat convection coefficient

5 Numerical simulation

5.1 Boundary conditions and loadings

In this hybrid modeling approach, equivalent thermomechanical loads are obtained and applied through experimentation and analytical models instead of simulating the time-consuming chip formation process, so the geometrical model is set with hole sizes. Meanwhile, to reduce the calculation time, a certain cutting depth of 5 mm is used instead of the whole depth 25.5 mm in order to reach the stable condition of thermomechanical loading, and the height of the model is set as 10 mm for the same purpose. To launch a simulation, parallel computation with 16 CPUs were used for running time of 1 week. The general boundary conditions of this model are shown as Fig. 11.

From Fig. 11, the outside parts and bottom of the workpiece are all fixed as they are restricted within the workpiece material, heat transfer within this area is regarded as a process occurred inside the material, and they are only slightly influenced by the deformation area due to the distance. Detailed descriptions of the heat transfer configuration will be introduced in "Sect. 5.2." For the top surface of the model, it has heat convection with air at room temperature, which has a heat convection coefficient of about 20 W/m^2•K. Plastic deformation will only occur within a very fine layer on the hole surface due to the

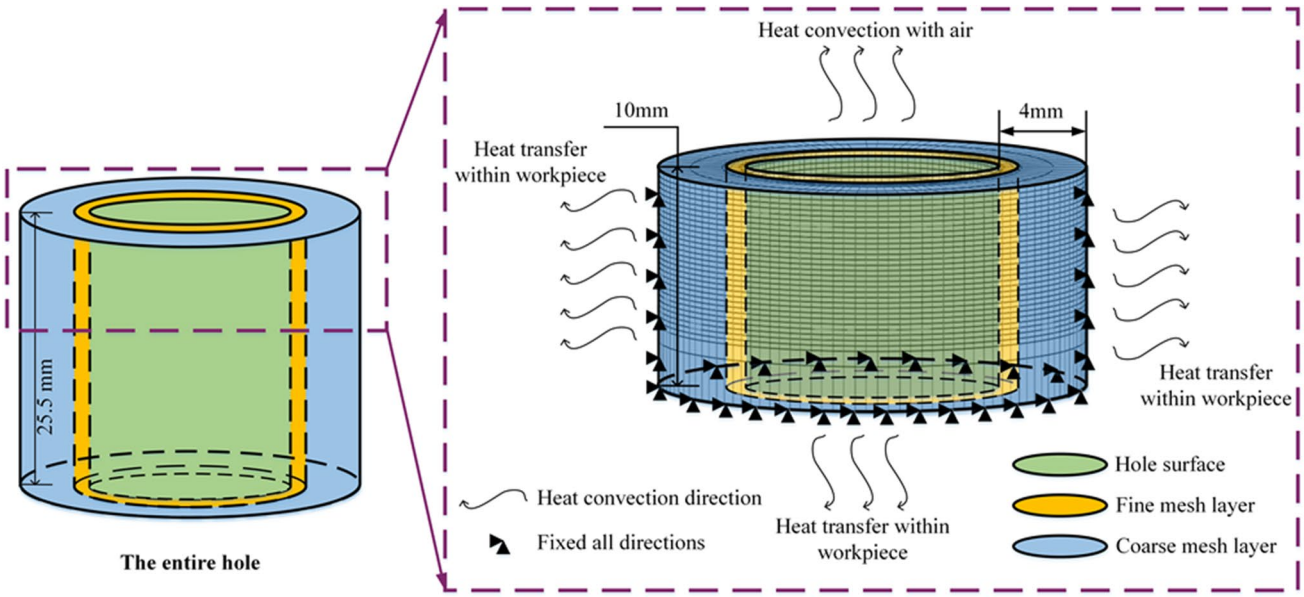

Fig. 11 Configuration of boundary conditions for numerical simulation

interaction between the drill and the workpiece, so plastic/elastic region is modeled separately with finer mesh, while elastic region with coarser mesh, in order to save the calculation time. The thickness of plastic layer is set as 1 mm in this study, while for the actual drilling process, the thickness of the layer with plastic deformation can be determined through the deformation of grains, which is less than 0.23 mm as shown in Fig. 12a) for dry cutting condition, which is measured by optical microscope on a sectioned sample of workpiece after metallographic preparation of mounting, etching, and polishing. As a result, the layer with finer meshes and plastic deformation is set with the thickness of 1 mm, which is higher than the largest thickness 0.23 mm obtained from experimental data and enough for simulation purpose, as plastic deformation will not occur outside this area.

The simulation was performed through the commercial software Abaqus/Standard, element types were used as C3D8RT due to the fully coupled thermomechanical process, and the finest mesh of 0.1 mm in the hole surface layer was used within the 1 mm thickness of plastic/elastic region. Mesh sensitivity was tested through purely thermal condition for a large size and a coupled thermomechanical condition for small size with drilling distance 1 mm and finest mesh 0.01 mm, respectively. The results show that the accuracy provided by finer meshes is not high enough with respect to the exponential increase in calculation time, and current mesh sizes show a good balance between calculation accuracy and efficiency. The material behavior described by the VPL model as illustrated in "Sect. 4.1" was programmed as a user-defined subroutine UHARD to be implemented into the simulation. Meanwhile, subroutine DLOAD was

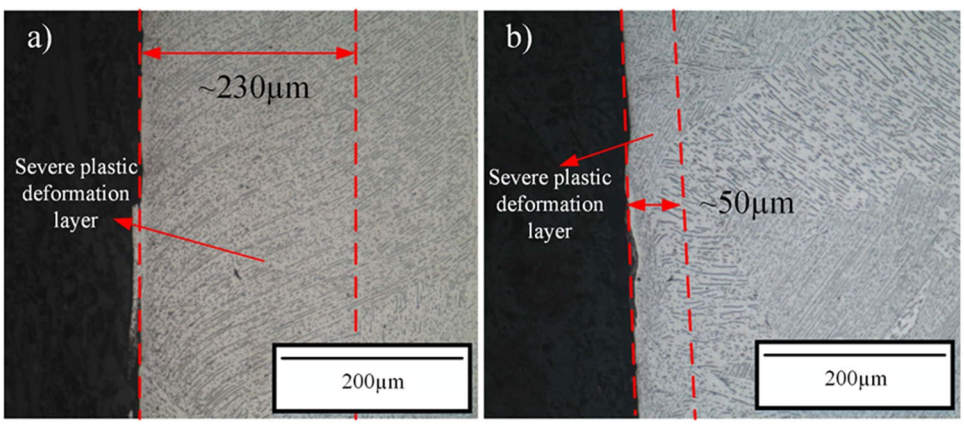

Fig. 12 Severe plastic deformation layer in hole surface under **a**) dry and **b**) cryogenic conditions with cutting speed 30 m/min and feed 0.08 mm/r

used to characterize normal pressure applied on hole surface and subroutine UTRACLOAD for shear stress. Moreover, subroutine DFLUX was used to describe the non-uniform distributed thermal loads applied on hole surface as calculated through the method proposed in "Sect. 4.3." For the loading procedures, they are all characterized along a helix path which is consistent with the real drilling process, and it can be expressed as variation of x-, y- and z-coordinates as follows:

$$x(t) = \frac{D}{2} \cdot \cos(-2\pi \cdot \frac{t}{T_N}) \tag{14}$$

$$y(t) = \frac{D}{2} \cdot \sin(-2\pi \cdot \frac{t}{T_N}) \tag{15}$$

$$z(t) = z_0 - f \cdot \frac{t}{T_N} \tag{16}$$

where D is the drill diameter, t the current time, and T_N the time required for a single rotation, z_0 is used to show the initial position of z-direction. When the distance between nodes and the trajectory described by Eqs. (14) ~ (16) lie within a certain value of w, which is the width of margin and equals to 0.85 mm in this study, the contact between drill and workpiece will occur and loads will be applied.

5.2 Heat transfer conditions

During drilling process, heat transfer will occur for workpiece material due to different contacts, which can be primarily attributed to three different pairs, which are drill and workpiece, air, and workpiece, and also cryogenic coolants with workpiece under cryogenic conditions, respectively. For precise description of heat transfer process by conventional cutting simulation, interactions between different phases like solids, liquids, and gases are essential to be implemented, which is very difficult and time-consuming. As a result, in this study, a developed description of heat transfer process between different materials and phases is implemented into the numerical simulation through a detailed characterization of heat convection coefficients. For this purpose, several assumptions require to be made in advance:

- Heat transfer between drill and workpiece is a solid-to-solid heat transfer. Therefore, as presented by Iqbal et al. [42], interfacial heat transfer coefficient between workpiece material and cutting tools used in machining simulations always fall within a large range of $1 \times 10^4 \sim 1 \times 10^8$ W/m^2•K in order to describe a perfect thermal conductance. Also, some lower coefficients ranging from $1 \times 10^3 \sim 1 \times 10^4$ W/m^2•K were reported by references [43–45] for titanium alloys, respectively. As a result, a sensitive test with coefficient ranging from $5 \times 10^3 \sim 1 \times 10^6$ W/m^2•K and inverse identification with experimental data were carried out, which shows the value of 1×10^6 W/m^2•K can present good results for both characterizations of temperature and displacements, and it was then used in this study.
- For dry cutting condition, the layer with removed materials and without tool contact will have heat convection with air.
- For cryogenic cutting condition, LN_2 will remain liquid phase when it contacts the workpiece material, and it will transform into gas phase as soon as the contact occurs. For liquid phase, the value of heat transfer coefficient can be characterized as illustrated in "Sect. 4.4," and for gas phase the value is referenced from literatures [18, 23] as 30 W/m^2•K, and the temperature for both gas and liquid phase nitrogen will be – 196 °C, the boiling temperature of LN_2.

Under these assumptions, the heat transfer conditions for both dry and cryogenic cutting can be described as Fig. 13.

In this study, cryogenic LN_2 was driven through the internal lubricant holes of the drill, which has a difference in phase angle with margin, as shown in Fig. 2; this phenomenon is implemented through user-defined subroutine FILM.

6 Results and discussions

6.1 Temperatures in hole surface

Drilling is a fully coupled thermomechanical process, and the key difference between dry cutting condition and cryogenic cutting condition is thermal effect, which can be well described through measuring temperatures. As illustrated in "Sect. 3," temperatures are measured through thermocouples installed with 1 mm distance away from hole surface and 5 mm away from the top surface, so the validation is carried out through the simulation results at the same position, as shown in Fig. 14.

A good agreement of temperature history has been obtained between simulation and experimental results for both dry and cryogenic cases, while the maximum values of temperatures are not reached due to the 5 mm distance away from the top surface. The maximum values of temperatures in simulation results and experimental data are validated as well, which shows a similar result with temperature around 200 °C. Figure 14 shows the comparison of temperature history, which does not reach the maximum due to the testing location and time, as temperature variation is time-dependent, while 5 s is not enough for this location in simulation. However, the highest temperature is reachable for higher locations as margin will pass them firstly and

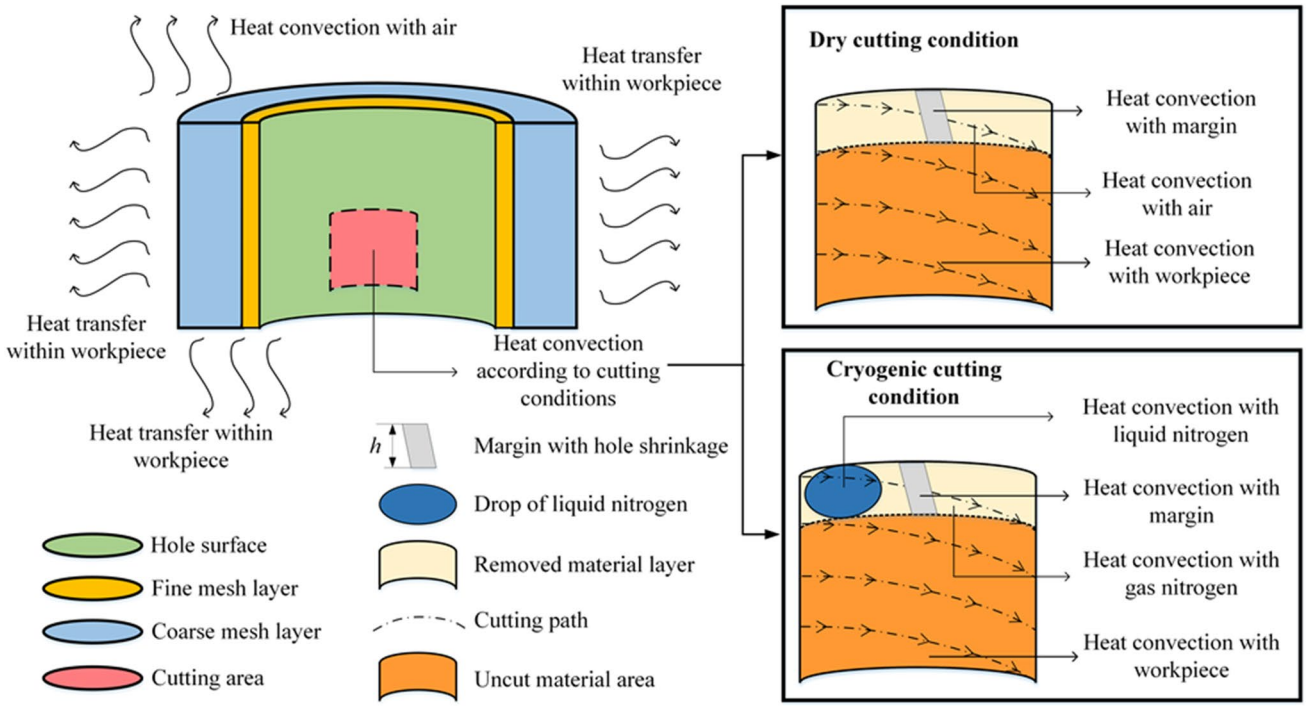

Fig. 13 Heat transfer conditions for dry and cryogenic cutting conditions

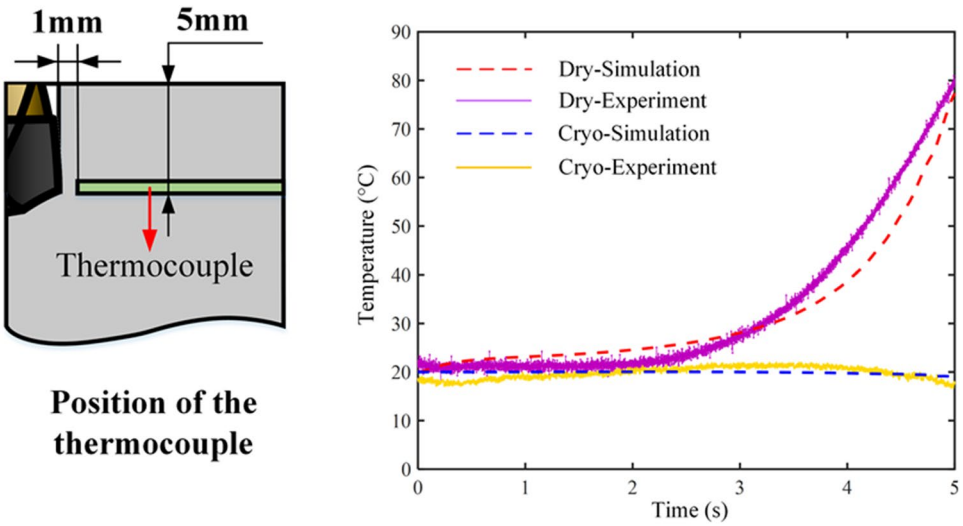

Fig. 14 Comparison of temperature between simulation results and experimental data for dry and cryogenic cutting conditions

Table 6 Experimental and numerical results of max/min temperatures under machined surface

	Dry condition (°C)			Cryogenic condition (°C)		
	Exp	Sim	Error	Exp	Sim	Error
Max	202.5	222.9	10.1%	28.4	25.6	9.9%
Min	——	——	——	−26.9	−29.6	10%

they have enough time for temperature to evolve; as a result, Table 6 presents the comparison of max/min temperatures between experimental results and numerical simulation, where minimum values show the lowest temperature induced by the cooling down through cryogenic coolants within the time period of 5 s.

Moreover, the locations for measuring temperature are 1 mm distance away from hole surface, and the actual temperature at exact surfaces is difficult to directly obtain during drilling process; as a result, simulation results are used to present these related data, as shown in Fig. 15, where the dotted lines show the same values as presented in Table 6. A discontinuous temperature distribution with a certain frequency is obtained, as heat flux can be regarded as a frequently distributed thermal load induced by drill margin, which shows a same frequency with respect to rotation speed. As a result, a thermal load will be applied on the surface when margin passes the related material point, so that a transient high temperature will be obtained, then it will decrease rapidly with the departure of the margin from this point, and finally turn into a stable value when the contact is finished. Meanwhile, the gap between surface temperature and temperature with distance is quite large, which is due to the extremely low thermal conductivity induced slow heat transfer speed and large temperature gradient.

Moreover, from Fig. 15, for dry condition, the transient temperatures on hole surfaces are extremely high, which will induce severe tool wear, while for cryogenic condition, the maximum value of transient temperatures on hole surface is less than 30% of that in dry cutting condition, and tool life will be significantly improved as the tool wear is primarily induced by thermal accumulation in drilling process. Meanwhile, temperatures will be soon transferred into negative under cryogenic cutting condition due to the continuous projection of LN_2 applied on hole surface; as a result, excessive heat will be brought away and related thermal expansion will be limited, so that heights of contact are decreased rapidly under cryogenic condition as reported by Merzouki et al. [15]. Moreover, with the rapid variation of temperature history and different temperature distribution between dry and cryogenic conditions, deformation mechanisms will be significantly changed as well, which will be discussed in following section.

6.2 Deformations along hole contour

During drilling process, the fully coupled thermomechanical loads applied on hole surface will induce elastic and plastic deformations, and plastic portion always leads to the permanent deformation, while elastic portion can show additional and excessive deformation and can be recovered from previous states. Moreover, during deformation, elastic portion can spring back and induce an additional interaction between cutting tool and workpiece with respect to the height of

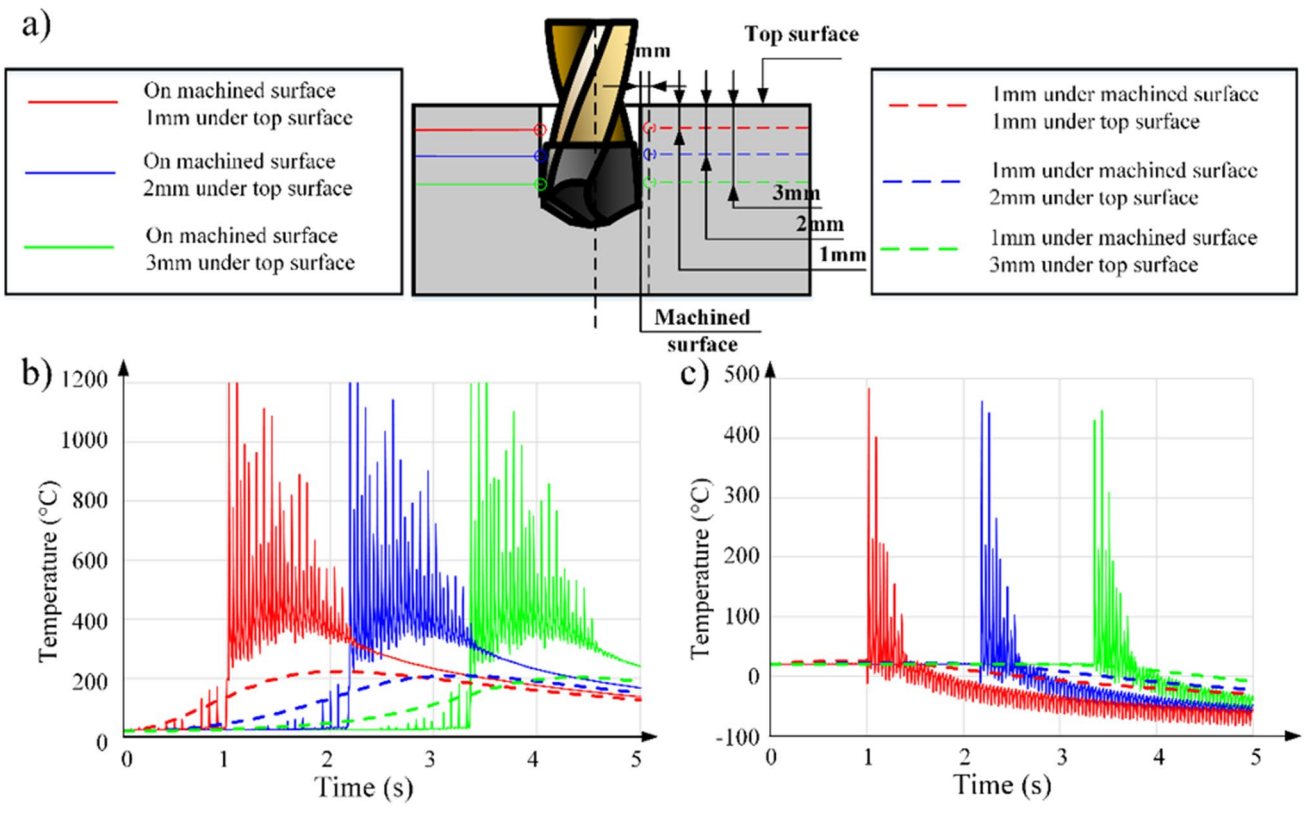

Fig. 15 Simulation results of temperature on hole surface at location with 1 mm under machined surface, **a** schematic for data acquisition, **b** temperature history of dry condition and **c** temperature history of cryogenic condition

contact; as a result, tool wear occurs rapidly and hole quality will be decreased under this condition. Therefore, limiting additional contact between tool and workpiece is essential in the improvement of tool wear and hole quality, which requires a deep understanding of the shrinkage mechanism and related deformation components. In this study, deformation components along hole contour are extracted during the whole drilling process in simulation through displacements of hole surfaces, as shown in Fig. 16.

For better description of the deformation history, variation of displacements along data acquisition line in Fig. 16 is further extracted with a time increment 0.05 s, which shows that the shrinkage is primarily induced by recoverable elastic deformation under cryogenic condition; however, for dry condition, it turns to elastoplastic deformation, as shown in Fig. 17.

In this study, the tool-workpiece contact is neglected in the model, as thermomechanical loads are directly applied on hole surface, which means that the displacements of hole contour are purely influenced by the loading condition without implementing the cutting tool. In Fig. 17, the path of drill movement is represented by the blue curve of perfect contour, and the displacements of hole contour are analyzed with the basement of this curve as well. Dotted curves represent the deformation history during the whole-drilling process, which are primarily consisted of elastic deformations, while the red curve represents the final curve with primary components of plastic deformation.

In the beginning of drilling process (as shown in Fig. 17 with $t = 1.0$ s), a similar deformation condition is obtained for both dry and cryogenic cases, as thermomechanical loads are still unstable at this stage. Meanwhile, the deformation obtained within this time step is even larger for cryogenic condition, which is due to the higher mechanical loads applied on related surface, as shown in Fig. 7, and the larger material volume of additional interaction under dry cutting condition is primarily due to the longer height of contact at this time step. However, with drilling process proceeding, deviations between dry and cryogenic cases become much larger. For cryogenic cases, the displacements with respect to the perfect contour are all positive, which means that expansion of materials is the dominant phenomenon under this condition, and the additional contact between tool and workpiece is primarily induced by the recovery of elastic deformation with a tiny volume. However, for dry cases, the displacements of final contour are always negative with respect to the perfect contour, showing that plastic deformation is also involved in the shrinkage phenomenon; as a result, the additional interaction between tool and workpiece is much more severe than that of cryogenic condition; meanwhile, the material volume of contact is also large due to the longer height of contact. Therefore, tool wear of margin under dry condition is more severe and the shape of hole contour will be influenced as well, which can be presented through cylindricity measured through the device Taylor Hobson Talyrond 585, as shown in Fig. 18.

For the experimental conditions shown in Fig. 18, cutting tests were stopped for dry cutting condition after 18 cuts when tool breakage occurs, and an obvious variation has been obtained for the hole contour. While for cryogenic condition, the tests were stopped after 63 cuts, and the hole contour still maintains unique with the drill showing a good performance. Meanwhile, the general tolerance of the hole is about 25 μm for cryogenic cutting condition, while it is increased to more than 45 μm for dry cutting condition. Besides additional interaction induced by hole shrinkage between cutting tool and workpiece as analyzed in previous paragraph, this enlargement of diameter can also be attributed to the initial tolerance of drill and formation of built-up edges (BUEs) [46], which will have a negative influence on surface quality. This kind of shrinkage occurs not only along the depth direction but also along the whole circle; in this

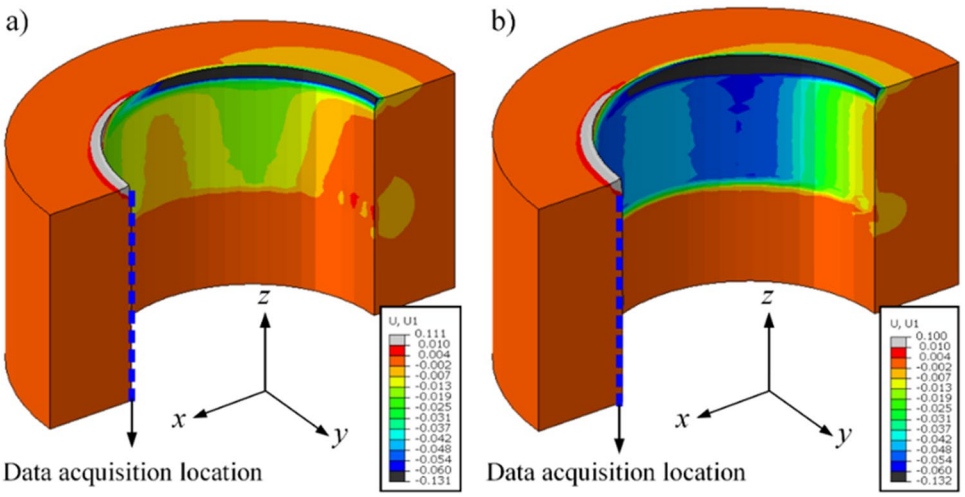

Fig. 16 Displacements along hole surfaces under different cooling conditions, **a**) dry and **b**) cryogenic

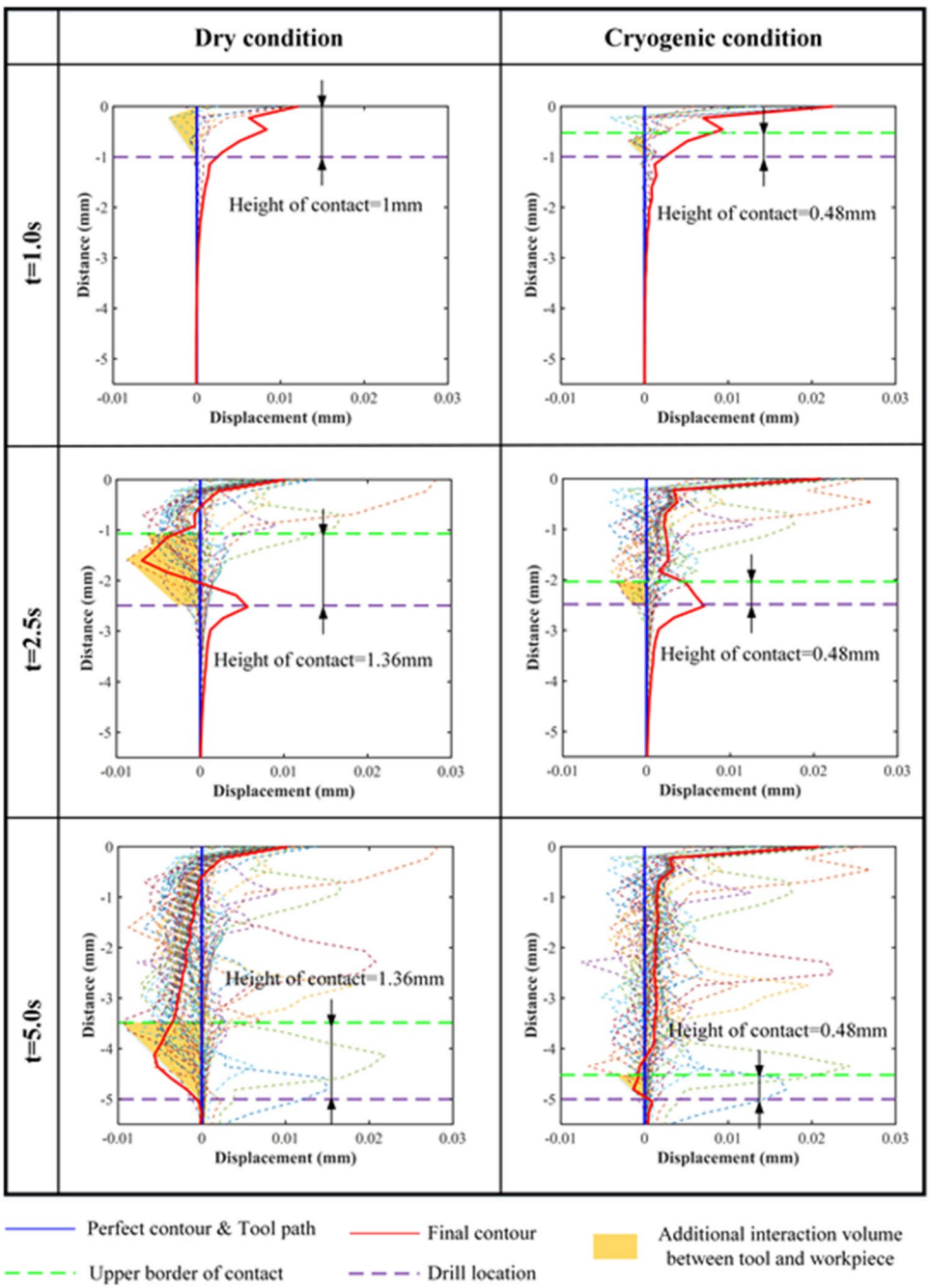

Fig. 17 Simulation results of deformation components and deformation history along hole contour during the whole drilling process under dry and cryogenic conditions, time increment between different deformation curves is 0.05 s

study, the circular coordinates with 2.5 mm beneath the top surface are extracted, as shown in Fig. 19.

From the perspective of simulation, the deformation along hole surface is not restricted by the contact with cutting tool, and it is performed with respect to the assumed perfect diameter 12 mm. For cryogenic condition, surface expansion is the dominant phenomenon with the maximum expanding distance of 3 μm, while for dry cutting condition, the key phenomenon is transferred into shrinkage with maximum shrinking distance 7 μm. The 3 μm expansion in cryogenic cutting condition can help to decrease the additional interaction between cutting tool and workpiece, while the 7 μm shrinkage in dry cutting condition will enhance the interaction, which will lead to the increase of tool wear and decrease of surface quality as a result.

Moreover, experimental data are also obtained with the same location; however, simulations are performed under the assumption of perfect contour with diameter 12 mm, which does not take the tolerances induced by drill geometry and BUEs into consideration; as a result, an average tolerance should be added to the simulation results in order to carry out the comparison of circular shapes with experimental

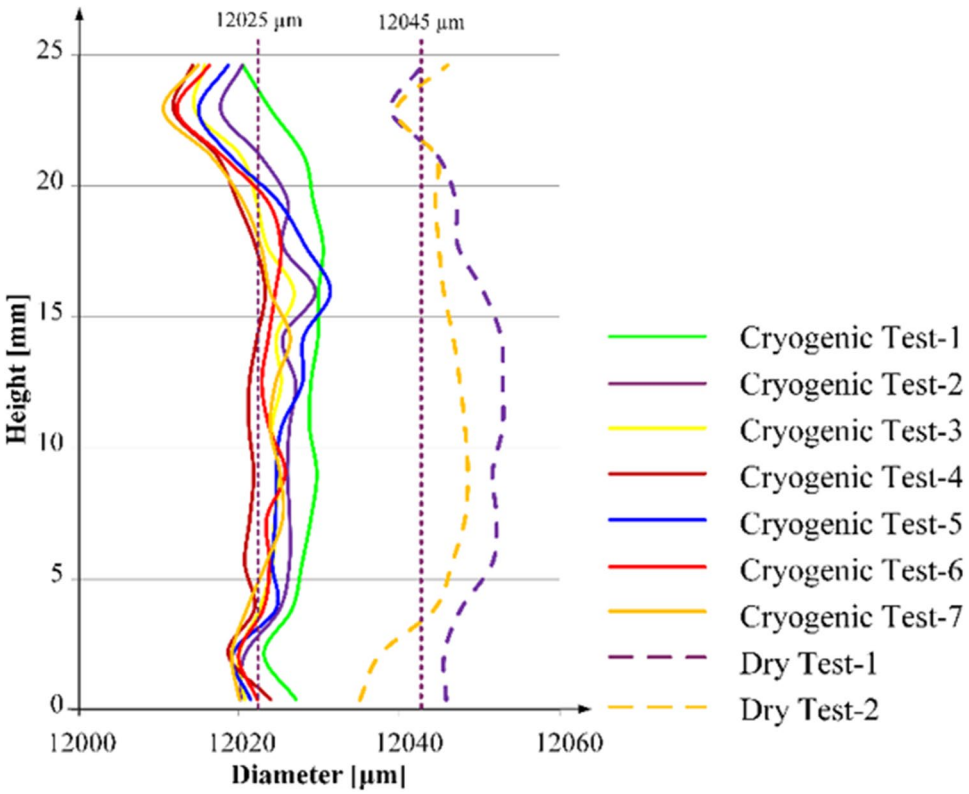

Fig. 18 Experimental data of hole contour under dry and cryogenic conditions [15]

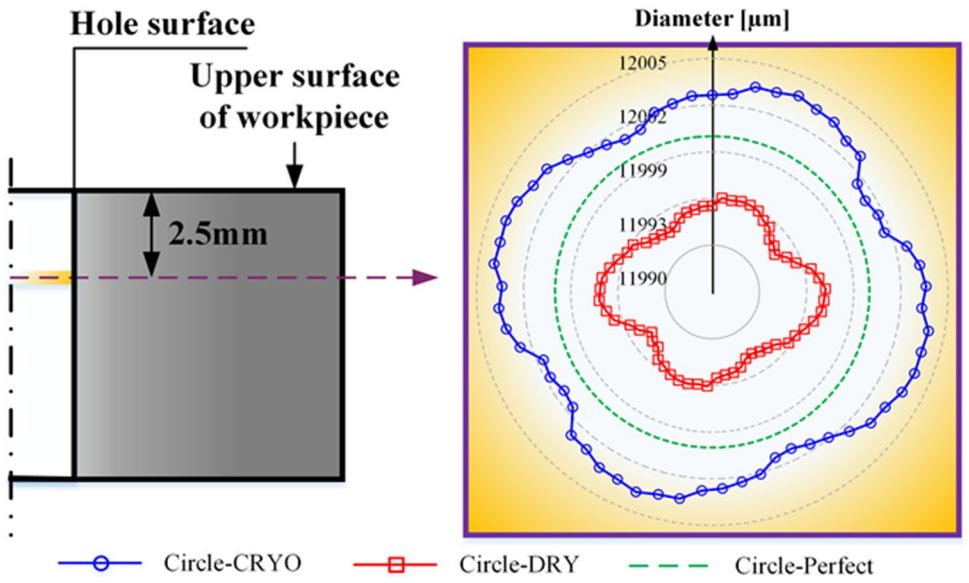

Fig. 19 Simulation results of circle shapes at 2.5 mm under top surface for dry and cryogenic cutting conditions

data, which is inversely identified from Fig. 18 as 25 µm for cryogenic condition and 45 µm for dry condition, respectively, and the results are as shown in Fig. 20.

With implementation of the geometrical and machining tolerances, a good agreement has been obtained between experimental data and simulation results; meanwhile, from experimental data, the fluctuation of the circle shape is more severe under dry cutting condition, which should be attributed to the shrinkage induced additional interaction between tool and workpiece as well. As a result, hole shrinkage induced negative displacements along hole contour, including both dimensions along depth direction and the circle shown from Fig. 17 to Fig. 20, can significantly increase the additional interaction between tool and workpiece material, which will lead to severe tool wear and poor surface quality, and cryogenic assistance is a good solution

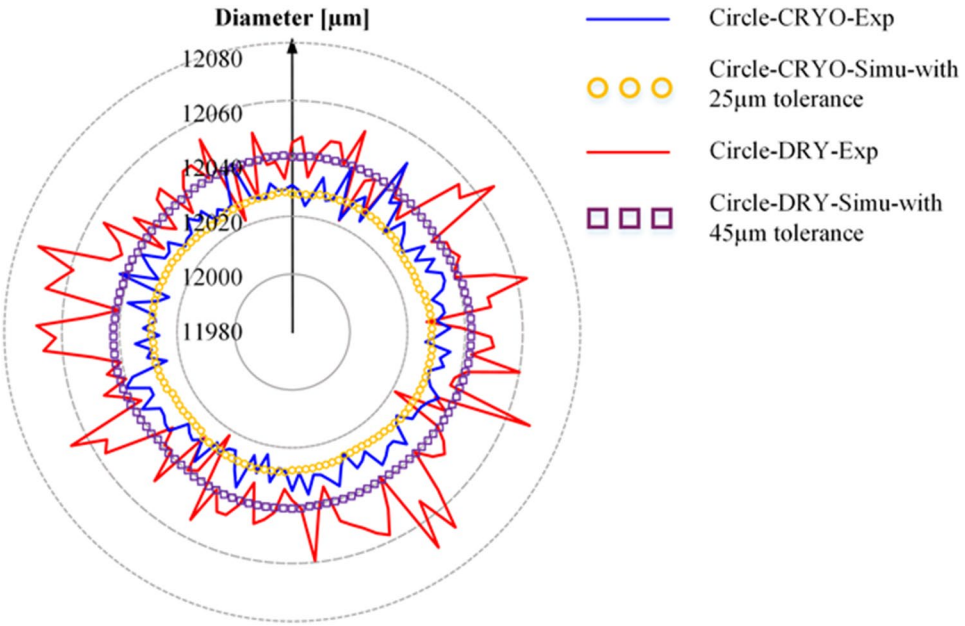

Fig. 20 Comparison of circle shapes between experimental data and simulation results at 2.5 mm under top surface for dry and cryogenic cutting conditions

to eliminate the shrinkage induced negative displacements in order to improve tool life and hole quality.

7 Conclusions

In this study, a hybrid modeling approach consisted of experimentation, analytical model, and numerical simulation is presented to characterize the hole shrinkage mechanism in drilling of Ti6Al4V under both dry and cryogenic cutting conditions, good agreements have been obtained between experimental data and simulation results, which performs an in-depth understanding of deformation states during the whole process in drilling, and conclusions can be drawn as followings:

- Hole shrinkage is primarily induced by variation of hole contour induced by elastoplastic deformation during drilling process, and elastic portion is a permanent part appearing in both dry and cryogenic conditions, as elastic deformation is always recoverable and prone to induce contact with workpiece material.
- Hole shrinkage induced by plastic deformation has a continuous influence on tool wear and surface integrity, which will decrease tool life and introduce damage to surface quality due to the decrease of cutting performance induced by the wear of margin, and it should be well prevented.
- Cryogenic assistance is an effective method in restricting plastic deformation induced hole shrinkage, as this portion is strongly dependent on thermal effects like thermal expansion, which can be well eliminated by cryogenic liquids as most heat will be brought by coolants and materials will show an opposite deforming direction at low temperatures.

This approach presents a potential for investigating surface integrity of machined parts with supply of coolants without applying complicated solid structure interaction process, which shows both good accuracy and high calculation efficiency.

Acknowledgements The authors would like to acknowledge Camille Robert from LAMPA, Arts et Métiers ParisTech Angers for his kind help in assistance of using the computational clusters.

Author contribution Hongguang Liu: methodology, data curation, formal analysis, validation, visualization, writing—original draft, reviewing & editing. Hélène Birembaux: Methodology, Data curation, Supervision, Writing – review & editing. Yessine Ayed: Methodology, Formal analysis, Supervision, Writing – review & editing. Frédéric Rossi: Validation, Data curation, Supervision, Writing – review & editing. Gérard Poulachon: Conceptualization, Funding acquisition, Project administration, Supervision, Writing – review & editing.

Funding This research was fully funded by Institute Carnot ARTS.

Data availability All data generated or analyzed during this study are included in this article.

Declarations

Consent to publish The authors consent that the work entitled as "A hybrid modelling approach for characterizing hole shrinkage mechanisms in drilling Ti6Al4V under dry and cryogenic conditions" for possible publication in International Journal of Advanced Manufacturing Technology. The authors certify that this manuscript is original and

has not been published in whole or in part nor is it being considered for publication elsewhere.

Competing interests The authors declare no competing interests.

References

1. Arrazola P-J, Garay A, Iriarte L-M, Armendia M, Marya S, Le Maître F (2009) Machinability of titanium alloys (Ti6Al4V and Ti555.3). J Mater Process Technol 209:2223–30. https://doi.org/10.1016/j.jmatprotec.2008.06.020
2. Rahman M, Wang Z-G, Wong Y-S (2006) A review on high-speed machining of titanium alloys. JSME Int J, Ser C 49:11–20. https://doi.org/10.1299/jsmec.49.11
3. Khanna N, Agrawal C, Gupta MK, Song Q (2020) Tool wear and hole quality evaluation in cryogenic Drilling of Inconel 718 superalloy. Tribol Int 143:106084. https://doi.org/10.1016/j.triboint.2019.106084
4. Poutord A, Rossi F, Poulachon G, M'Saoubi R, Abrivard G (2013) Local Approach of wear in drilling Ti6Al4V/CFRP for stack modelling. Procedia CIRP 8:316–321. https://doi.org/10.1016/j.procir.2013.06.109
5. Merzouki J, Poulachon G, Rossi F, Ayed Y, Abrivard G (2017) Method of hole shrinkage radial forces measurement in Ti6Al4V drilling. Procedia CIRP 58:629–634. https://doi.org/10.1016/j.procir.2017.03.226
6. Abdelhafeez AM, Soo SL, Aspinwall DK, Dowson A, Arnold D (2015) Burr Formation and hole quality when drilling titanium and aluminium alloys. Procedia CIRP 37:230–235. https://doi.org/10.1016/j.procir.2015.08.019
7. Uehara K, Kumagai S (1968) Chip formation, surface roughness and cutting force in cryogenic machining. Ann CIRP 17:68–74
8. Hong SY, Ding Y (2001) Cooling approaches and cutting temperatures in cryogenic machining of Ti-6Al-4V. Int J Mach Tools Manuf 41:1417–1437. https://doi.org/10.1016/S0890-6955(01)00026-8
9. Hong SY, Ding Y, Jeong W (2001) Friction and cutting forces in cryogenic machining of Ti–6Al–4V. Int J Mach Tools Manuf 41:2271–2285. https://doi.org/10.1016/S0890-6955(01)00029-3
10. Hong SY, Markus I, Jeong W (2001) New cooling approach and tool life improvement in cryogenic machining of titanium alloy Ti-6Al-4V. Int J Mach Tools Manuf 41:2245–2260. https://doi.org/10.1016/S0890-6955(01)00041-4
11. Mia M, Gupta MK, Lozano JA, Carou D, Pimenov D, Królczyk G et al (2019) Multi-objective optimization and life cycle assessment of eco-friendly cryogenic N2 assisted turning of Ti-6Al-4V. J Clean Prod 210:121–33. https://doi.org/10.1016/j.jclepro.2018.10.334
12. Jawahir IS, Attia H, Biermann D, Duflou J, Klocke F, Meyer D et al (2016) Cryogenic manufacturing processes. CIRP Ann 65:713–736. https://doi.org/10.1016/j.cirp.2016.06.007
13. Ayed Y, Germain G, Melsio AP, Kowalewski P, Locufier D (2017) Impact of supply conditions of liquid nitrogen on tool wear and surface integrity when machining the Ti-6Al-4V titanium alloy. Int J Adv Manuf Technol 93:1199–1206. https://doi.org/10.1007/s00170-017-0604-7
14. Stampfer B, Golda P, Schießl R, Maas U, Schulze V (2020) Cryogenic orthogonal turning of Ti-6Al-4V: analysis of nitrogen supply pressure variation and subcooler usage. Int J Adv Manuf Technol 111:359–369. https://doi.org/10.1007/s00170-020-06105-z
15. Merzouki J, Poulachon G, Rossi F, Ayed Y, Abrivard G (2020) Effect of cryogenic assistance on hole shrinkage during Ti6Al4V drilling. Int J Adv Manuf Technol 108:2675–2686. https://doi.org/10.1007/s00170-020-05381-z
16. Kaynak Y, Gharibi A (2019) Cryogenic machining of titanium Ti-5553 Alloy. J Manuf Sci Eng 141:041012. https://doi.org/10.1115/1.4042605
17. Shokrani A, Dhokia V, Newman ST (2016) Investigation of the effects of cryogenic machining on surface integrity in CNC end milling of Ti–6Al–4V titanium alloy. J Manuf Process 21:172–179. https://doi.org/10.1016/j.jmapro.2015.12.002
18. Pusavec F, Lu T, Courbon C, Rech J, Aljancic U, Kopac J et al (2016) Analysis of the influence of nitrogen phase and surface heat transfer coefficient on cryogenic machining performance. J Mater Process Technol 233:19–28. https://doi.org/10.1016/j.jmatprotec.2016.02.003
19. Guo W, Pei Z, Sang X, Poplawsky JD, Bruschi S, Qu J et al (2019) Shape-preserving machining produces gradient nanolaminate medium entropy alloys with high strain hardening capability. Acta Mater 170:176–186. https://doi.org/10.1016/j.actamat.2019.03.024
20. Liu H, Zhang J, Xu B, Xu X, Zhao W (2020) Prediction of microstructure gradient distribution in machined surface induced by high speed machining through a coupled FE and CA approach. Mater Des 196:109133. https://doi.org/10.1016/j.matdes.2020.109133
21. Salame C, Bejjani R, Marimuthu P (2019) A better understanding of cryogenic machining using CFD and FEM simulation. Procedia CIRP 81:1071–1076. https://doi.org/10.1016/j.procir.2019.03.255
22. Rotella G, Umbrello D (2014) Finite element modeling of microstructural changes in dry and cryogenic cutting of Ti6Al4V alloy. CIRP Ann 63:69–72. https://doi.org/10.1016/j.cirp.2014.03.074
23. Dix M, Wertheim R, Schmidt G, Hochmuth C (2014) Modeling of drilling assisted by cryogenic cooling for higher efficiency. CIRP Ann 63:73–76. https://doi.org/10.1016/j.cirp.2014.03.080
24. Imbrogno S, Sartori S, Bordin A, Bruschi S, Umbrello D (2017) Machining simulation of Ti6Al4V under dry and cryogenic conditions. Procedia CIRP 58:475–480. https://doi.org/10.1016/j.procir.2017.03.263
25. Umbrello D, Bordin A, Imbrogno S, Bruschi S (2017) 3D finite element modelling of surface modification in dry and cryogenic machining of EBM Ti6Al4V alloy. CIRP J Manuf Sci Technol 18:92–100. https://doi.org/10.1016/j.cirpj.2016.10.004
26. Shi B, Elsayed A, Damir A, Attia H, M'Saoubi R (2019) A hybrid modeling approach for characterization and simulation of cryogenic machining of Ti–6Al–4V alloy. J Manuf Sci Eng 141:021021. https://doi.org/10.1115/1.4042307
27. Valiorgue F, Rech J, Hamdi H, Gilles P, Bergheau JM (2007) A new approach for the modelling of residual stresses induced by turning of 316L. J Mater Process Technol 191:270–273. https://doi.org/10.1016/j.jmatprotec.2007.03.021
28. Valiorgue F, Rech J, Hamdi H, Gilles P, Bergheau JM (2012) 3D modeling of residual stresses induced in finish turning of an AISI304L stainless steel. Int J Mach Tools Manuf 53:77–90. https://doi.org/10.1016/j.ijmachtools.2011.09.011
29. Mondelin A, Valiorgue F, Rech J, Coret M, Feulvarch E (2012) Hybrid model for the prediction of residual stresses induced by 15–5PH steel turning. Int J Mech Sci 58:69–85. https://doi.org/10.1016/j.ijmecsci.2012.03.003
30. Ramirez C (2017) Critères d'optimisation des alliages de TITane pouraméliorer leur USinabilité. ENSAM, Paris
31. Follansbee PS, Gray GT (1989) An analysis of the low temperature, low and high strain-rate deformation of Ti-6AI-4V. Metall Trans A 20(5):863–874. https://doi.org/10.1007/BF02651653
32. Mills KC (2002) Recommended values of thermophysical properties for selected commercial alloys. Woodhead Publishing
33. Swarnakar AK, Van der Biest O, Baufeld B (2011) Thermal expansion and lattice parameters of shaped metal deposited

Ti–6Al–4V. J Alloy Compd 509:2723–2728. https://doi.org/10.1016/j.jallcom.2010.12.014
34. Marquardt ED, Le JP, Radebaugh R (2002) Cryogenic material properties database. Cryocoolers 11, Springer, p 681–7
35. Ziegler WT, Mullins JC, Hwa SCP (1963) Specific heat and thermal conductivity of four commercial titanium alloys from 20 to 300 K. Advances in Cryogenic Engineering, Springer, p 268–77
36. Faverjon P, Rech J, Valiorgue F, Orset M (2015) Optimization of a drilling sequence under MQL to minimize the thermal distortion of a complex aluminum part. Prod Eng Res Devel 9:505–515. https://doi.org/10.1007/s11740-015-0614-y
37. Shi G, Deng X, Shet C (2002) A finite element study of the effect of friction in orthogonal metal cutting. Finite Elem Anal Des 38:863–883
38. Rech J, Arrazola PJ, Claudin C, Courbon C, Pusavec F, Kopac J (2013) Characterisation of friction and heat partition coefficients at the tool-work material interface in cutting. CIRP Ann 62:79–82. https://doi.org/10.1016/j.cirp.2013.03.099
39. Courbon C, Pusavec F, Dumont F, Rech J, Kopac J (2013) Tribological behaviour of Ti6Al4V and Inconel718 under dry and cryogenic conditions—application to the context of machining with carbide tools. Tribol Int 66:72–82. https://doi.org/10.1016/j.triboint.2013.04.010
40. Lequien P, Poulachon G, Outeiro JC, Rech J (2018) Hybrid experimental/modelling methodology for identifying the convective heat transfer coefficient in cryogenic assisted machining. Appl Therm Eng 128:500–507. https://doi.org/10.1016/j.applthermaleng.2017.09.054
41. Lequien P (2017) Etude fondamentale de l'assistance cryogénique pour application au fraisage du Ti6Al4V. ENSAM, Paris
42. Iqbal SA, Mativenga PT, Sheikh MA (2008) An investigative study of the interface heat transfer coefficient for finite element modelling of high-speed machining. Proc Inst Mech Eng B J Eng Manuf 222:1405–1416. https://doi.org/10.1243/09544054JEM1179
43. Liu X, Kopec M, El Fakir O, Qu H, Wang Y, Wang L et al (2020) Characterisation of the interfacial heat transfer coefficient in hot stamping of titanium alloys. Int Commun Heat Mass Transfer 113:104535. https://doi.org/10.1016/j.icheatmasstransfer.2020.104535
44. Lu B, Wang L, Geng Z, Huang Y (2017) Determination of interfacial heat transfer coefficient for TC11 titanium alloy hot forging. Heat Mass Transfer 53:3049–3058. https://doi.org/10.1007/s00231-017-2032-5
45. Xu M, Ling R, Zhang Z, Xie J (2017) Study on interfacial heat transfer behavior of TA15 titanium alloy and die materials. Int J Heat Mass Transf 108:1573–1578. https://doi.org/10.1016/j.ijheatmasstransfer.2016.12.078
46. Zhu Z, Guo K, Sun J, Li J, Liu Y, Zheng Y et al (2018) Evaluation of novel tool geometries in dry drilling aluminium 2024–T351/titanium Ti6Al4V stack. J Mater Process Technol 259:270–281